Journal of Materials Chemistry C

PAPER

View Article Online
View Journal | View Issue

Cite this: J. Mater. Chem. C, 2015, 3, 10215

Peripheral *versus* axial substituted phthalocyanine-double-walled carbon nanotube hybrids as light harvesting systems†

Luis M. Arellano,[a] Luis Martín-Gomis,[b] Habtom B. Gobeze,[c] Myriam Barrejón,[a] Desiré Molina,[b] María J. Gómez-Escalonilla,[a] José Luis G. Fierro,[d] Minfang Zhang,[e] Masako Yudasaka,[e] Sumio Iijima,[e] Francis D'Souza,*[c] Fernando Langa*[a] and Ángela Sastre-Santos*[b]

Received 13th July 2015,
Accepted 2nd September 2015

DOI: 10.1039/c5tc02114f

www.rsc.org/MaterialsC

Selective functionalization of the outer walls of double-walled carbon nanotubes (DWCNTs) with zinc and silicon phthalocyanines leaving the inner walls undamaged has been accomplished. The mode of metal phthalocyanine (MPc) connection was varied, that is, through the macrocycle periphery in the case of zinc phthalocyanines (ZnPcs) and through the silicon axial position in the case of silicon phthalocyanines (SiPcs) to visualize its effect on phthalocyanine–DWCNT interactions. Evidence of outer wall functionalization and the degree of phthalocyanine substitution on DWCNTs were arrived from HR-TEM, AFM, TGA, XPS and Raman techniques. The sensitizer-nanotube interactions were probed from studies involving optical absorbance, steady-state and time resolved emission, and electrochemical studies. The fluorescence of phthalocyanines in these hybrids was found to be almost quantitatively quenched (>95%) due to the interactions with DWCNTs, and such interactions were more for the SiPc derived hybrids. The femtosecond transient absorption studies performed revealed that the interactions are dynamic involving the singlet excited phthalocyanines and the nanotubes. In agreement with earlier studies, evidence for charge separation in these hybrids was bleak revealing weak signature bands of $MPc^{\bullet+}$ in the 850 nm range. Additionally, the presence of trace amounts of single-walled carbon nanotubes in the hybrids further hampered detailed spectral analysis.

Introduction

The use of carbon nanostructures, as principal components in donor–acceptor nanoensembles, is now experiencing a new impulse, primarily due to the actual momentum around graphene and graphene-based materials, but also because of current multi-gram availability of fine structure-controlled nanotube batches.[1] Carbon nanotubes (CNTs) have always been considered as a very promising class of carbon-based building blocks, suitable to construct hybrid materials with exceptional optoelectronic features, but the historic variability between batches has been, until now, a handicap that should be eluded in near future to afford their reliable employment in organic-based technological applications.[2] In spite of that, very interesting hybrid materials, based on the smart combination of electron donor counterparts and CNTs, either by a classical covalent method[3] or a non-covalent interaction, have been described.[4] Nevertheless, neither of the strategies is perfect: while covalent bonding provides robust hybrid materials at the cost of sacrificing electronic properties, the supramolecular approach provides hybrids that are not very stable although this approach yields materials without introducing defects on the conjugated sp^2 carbon lattice.

Double-walled carbon nanotubes (DWCNTs),[5] due to the electronic communication between outer and inner walls,[6] have recently emerged out as a convenient substitute for functionalized CNT hybrid materials as they combine all of the advantages found in the covalent and the supramolecularly

[a] Universidad de Castilla-La Mancha, Instituto de Nanociencia, Nanotecnología y Materiales Moleculares (INAMOL), 45071-Toledo, Spain. E-mail: Fernando.Langa@uclm.es
[b] Área de Química Orgánica, Instituto de Bioingeniería, Universidad Miguel Hernández, Avda. de la Universidad, s/n, Elche 03202, Spain. E-mail: asastre@umh.es
[c] Chemistry and Materials Science and Engineering, University of North Texas, 76203-5017 Denton, TX, USA. E-mail: Francis.DSouza@UNT.edu
[d] Instituto de Catálisis y Petroleoquímica, CSIC, Cantoblanco, 28049, Madrid, Spain. E-mail: jlgfierro@icp.csic.es
[e] Nanotube Research Center, National Institute of Advanced Industrial Science and Technology, Higashi, Tsukuba, Ibaraki 305-8565, Japan

† Electronic supplementary information (ESI) available: Synthesis and characterization of reference Pcs, experimental details, electrochemistry and nanosecond flash photolysis results. See DOI: 10.1039/c5tc02114f

functionalized hybrids. This strategy has been recently explored by us for the first time using perylenediimides (PDIs) as electron donor decorating agents, obtaining a series of DWCNT–PDI hybrids[7a] and more recently with antibodies.[7b] However, although we were able to detect an effective electronic communication between inner and outer DWCNT walls where the inherent fluorescence of the PDI subunit was effectively quenched, the evidence of charge separation from the transient studies was bleak, and accordingly, yields of photocatalytic electron pooling were much lower than those reported earlier for fullerene and single-walled carbon nanotube based hybrids.

In this work we present DWCNTs covalently linked to good electron donor systems wherein we have been able to observe strong intramolecular interactions. We have chosen phthalocyanines (Pcs),[8] robust electron rich systems capable of forming long lived charge separated states,[9] to synthesize two new DWCNT hybrids, **DWCNT–ZnPc 1** and **DWCNT–SiPc 2** (Chart 1). Moreover, we have studied the influence of the π-conjugate linker's effect on the DWCNT–Pc interactions using fully conjugated peripherally substituted zinc phthalocyanines and non-conjugated axially substituted silicon phthalocyanines. The structural properties of both DWCNT–phthalocyanine hybrids have been investigated *via* thermogravimetric analysis (TGA), X-ray photoelectron (XPS), Raman spectroscopies, transmission electron (TEM) and atomic force (AFM) microscopies. The photophysical properties of the DWCNT–Pc's derivatives have been studied by absorption and emission spectroscopic techniques in solution. This study is targeted to shed light on the electronic interactions between the electron donor phthalocyanine connected *via* conjugated and non-conjugated means to the outer wall of DWCNTs, and its conducting inner tube. In these DWCNT–Pc hybrids, the inner tube would keep its (ideal) ballistic conducting behavior, being capable of rapidly transporting an electron to an external circuit, generated during the photoexcitation of the Pcs, to be incorporated in the future in highly efficient solar cells.

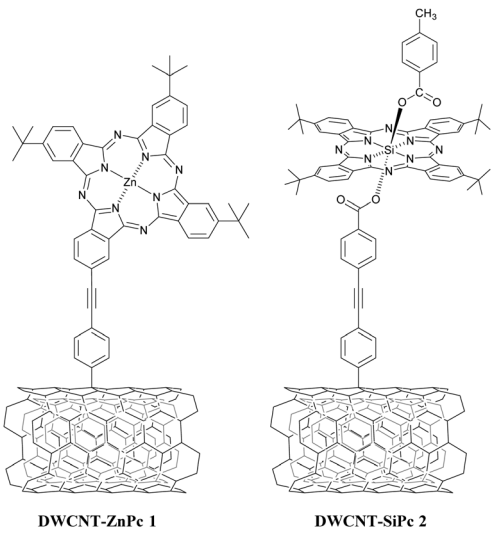

Chart 1 Structure of **DWCNT–ZnPc 1** and **DWCNT–SiPc 2**.

Results and discussion

Synthesis and characterization

The synthetic procedure for the preparation of the corresponding **DWCNT–ZnPc 1** and **DWCNT–SiPc 2** is illustrated in Scheme 1. Initially, pristine DWCNT was covalently functionalized by Tour reaction[10] with 4-(2-trimethylsilyl)ethynylaniline in the presence of isoamyl nitrite affording **DWCNT–TMS**. Subsequent cleavage of the TMS groups using tetra-*n*-butylammonium fluoride (TBAF) gave **DWCNT–CCH**. Finally, **ZnPc 3** and **SiPc 4** were grafted onto the modified DWCNTs using a Sonogashira C–C cross coupling reaction[11] affording the targeted nanohybrids **1** and **2**.

ZnPc 3 was obtained following a previously described procedure,[12] while asymmetric diaxially-substituted **SiPc 4** was synthesized, for the first time, from tetra-*tert*-butyl silicon dichlorophthalocyanine,[13] and equimolar quantities of 4-iodobenzoic acid and 4-methylbenzoic acid (Scheme 2) using, in this

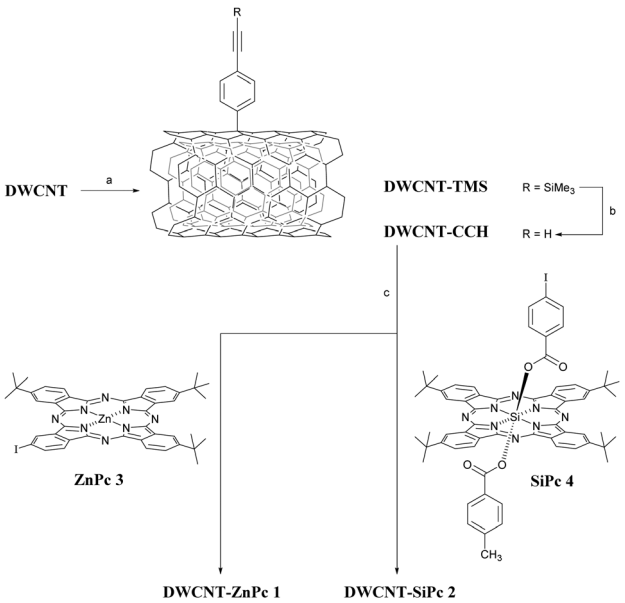

Scheme 1 *Reagents and conditions*: (a) 4-[(2-trimethylsilyl)ethynyl]-aniline, isoamyl nitrite, NMP, 70 °C, 24 h; (b) TBAF, 0 °C to rt, 3 h; (c) then, **Pc 3** or **Pc 4**, $Pd_2(dba)_3$, $AsPh_3$, NEt_3, DMF, 120 °C, 4 days.

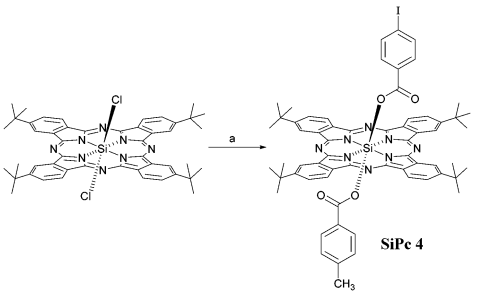

Scheme 2 *Reagents and conditions*: (a) 4-iodobenzoic acid, 4-methylbenzoic acid, 1-butyl-3-methylimidazolium bromide, diglyme, microwave irradiation (200 M_W, 200 W, 15 min).

case, microwave radiation to force double chloride substitution at the axial valences (see ESI† for Experimental details).

Despite that ZnPcs are a good reference compound, we have also included Zn(II) tri(*tert*-butyl-4-(1′-phenyl)ethynyl) phthalocyanine (**ZnPc 5**) as reference to get a more accurate study of the influence of the interactions of the ZnPcs over the DWCNTs and *vice versa*, ruling out the effect of the phenylethynyl bridge in the ground state electronic and redox properties of hybrid **1**. **ZnPc 5** was synthesized (Scheme 3) following a modified synthetic route to the already published.[14] Sonogashira coupling of (tri-*tert*-butyl-ethynylphthalocyaninato)zinc(II)[12] with bromobenzene afforded **ZnPc 5** in 50% yield (see ESI†).

DWCNT–Pc nanoconjugates **1** and **2** were characterized by Raman spectroscopy, thermogravimetric analysis (TGA), UV-vis absorption, X-ray photoelectron spectroscopy (XPS), transmission electron microscopy (TEM) and atomic force microscopy (AFM) as well as steady-state and time-resolved spectroscopic techniques to obtain fully detailed information about the structural, electronic and chemical properties of the functionalized double-walled carbon nanotubes.

Thermogravimetric analysis (TGA) was applied to detect the degree of functionalization of the functionalized samples under an inert atmosphere and at 600 °C. The thermogram shown in Fig. 1 revealed a weight loss about 4.1% for pristine **DWCNT**, 16.6% for **DWCNT–TMS**, 20.5% for phthalocyanine hybrid **DWCNT–ZnPc 1** and 51.2% for the control phthalocyanine **ZnPc 3**. The corrected weight losses due to the functional groups on nanotubes were then estimated to be 12.5% for **DWCNT–TMS** and about 16.4% for nanohybrid **1** (weight loss difference of **DWCNT–TMS** – pristine **DWCNT** and **DWCNT–ZnPc 1** – pristine **DWCNT**). Accordingly, a degree of functionalization of one unit of organic fragments per about 110 carbon atoms for **DWCNT–TMS** could be estimated; with the same calculation, the amount of functional groups was 1 per 362 carbon atoms in nanohybrid **1**.

In the case of nanohybrid **2**, the thermogravimetric analysis revealed a corrected weight loss of 14.2%, 19.8% and 51.5% (for **DWCNT–TMS**, **DWCNT–SiPc 2** and **SiPc 4** respectively). According to these results, the number of organic addends in **DWCNT–TMS** was estimated as 1 per 98 carbon atoms and every 411 carbon atoms in **DWCNT–SiPc 2** (Fig. 2). The weight loss of 4.1% at 600 °C observed for pristine DWCNTs may be due to the destruction of the residual amorphous carbon still present in the nanotubes and to the decarboxylation of the oxidized species.

The functionalization procedure was also monitorized by X-ray photoelectron spectroscopy (XPS). The binding energies of core levels of the elements and percentage of peak components of both **DWCNT–Pcs** and some of the raw reagents are summarized in Table S1 (see ESI†). Also included in this table are the BEs of core-levels of the elements of pristine DWCNTs with those of **Pcs** (**ZnPc 3** and **SiPc 4**) and **DWCNT–TMS** intermediates employed in the synthesis of **DWCNT–Pcs**.

Fitting of the high resolution C 1s spectrum of the pristine DWCNT sample (Fig. S7 in ESI†) displayed the main component at 284.8 eV, due to sp^2 C on the DWCNT surface, and other minor components at 286.2, 287.7 and 289.2 eV assigned to C–O, C=O and COO groups respectively.[15] Moreover, this C 1s line shows a broad, weak component at about 291.3 eV, originating from the π–π* plasmon emission of C atoms in graphene-like structures.[16] Similarly, the high resolution O 1s peak of DWCNTs has been resolved with two components at 531.8 and 533.3 eV originating from O=C and O–C bonds present on the DWCNT surface.[17]

Upon anchoring the TMS group to DWCNT substrates, some changes in the C 1s profile were observed: a minor contribution appeared at 285.3 eV, coming from the sp^3 C of the TMS group (see Fig. S8, ESI†), and simultaneously the π–π* plasmon emission disappeared. Quantitative data have also been obtained

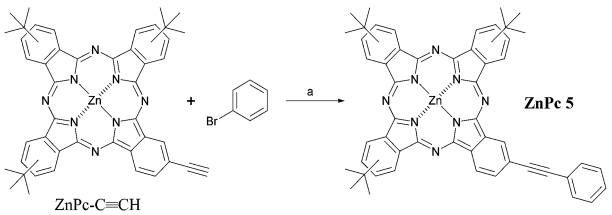

Scheme 3 *Reagents and conditions*: (a) $Pd(PPh_3)_4$, CuI, THF, Et_3N, Ar, 50 °C, 90 min.

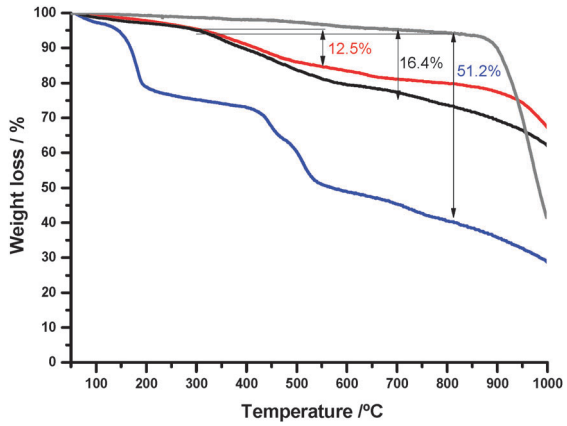

Fig. 1 TGA curves of pristine **DWCNT** (grey), **DWCNT–TMS** (red), **DWCNT–ZnPc 1** (black) and **ZnPc 3** (blue), (10 °C min^{-1} under nitrogen).

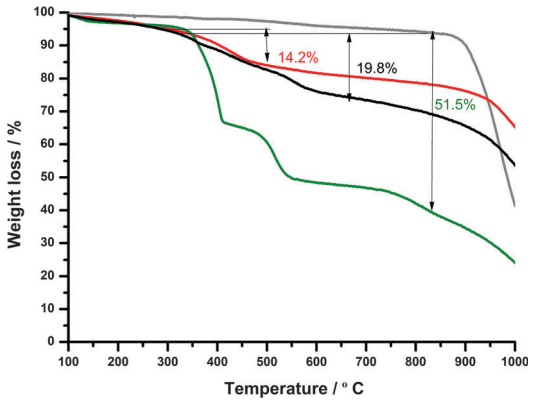

Fig. 2 TGA profiles of pristine **DWCNT** (grey), **DWCNT–TMS** (red), **DWCNT–SiPc 2** (black) and **SiPc 4** (green), (10 °C min^{-1} under nitrogen).

Table 1 XPS elemental composition of pristine DWCNTs, functionalized DWCNT samples and their precursors

Sample	C (at%)	O (at%)	N (at%)	Si (at%)	Zn (at%)	I (at%)
ZnPc 3	84.6	—	12.5	—	1.4	1.5
SiPc 4	77.7	6.6	12.2	1.7	—	1.8
pristine **DWCNT**	95.1	4.9	—	—	—	—
DWCNT–TMS	96.3	3.1	—	0.6	—	—
DWCNT–ZnPc 1	93.3	3.0	3.3	—	0.4	—
DWCNT–SiPc 2	92.0	4.6	3.0	0.4	—	—

from XPS spectra. Surface composition of pristine DWCNTs in terms of atom percentage is compiled in Table 1. The O-content of the pristine DWCNTs is moderate (4.9%) and becomes reduced to 3.1% upon incorporation of TMS groups indicating that the anchorage of TMS groups removes some of the O-containing groups of the pristine DWCNTs.

In addition, the BE values of **DWCNT–Pcs 1** and **2**, and corresponding **ZnPc 3** and **SiPc 4** precursors are also summarized in Table S1 (ESI†). C 1s and O 1s emissions of **1** and **2** display contributions of both substrate and phthalocyanine precursors, together with N 1s and Zn 2p and Si 2p peaks originating from the phthalocyanine moieties. The N 1s peak of these functionalized samples was satisfactorily fitted to two components: the lower BE (398.7–398.8 eV) corresponding to six imine nitrogen atoms, while the peak at higher BE (400.3 eV) is associated with the two pyrrolic nitrogen atoms;[18] the former peak is three times more intense than the latter. This observation is consistent with the molecular anchoring of the phthalocyanine moiety on the DWCNT substrates (see Table S1, ESI†).

As shown in Table 1, indirect evidence for functionalization of the DWCNTs with phthalocyanine groups comes from comparing atom percentages of C, O, N and Zn or Si in functionalized DWCNT samples. The similar Zn and Si percentage (0.4%) in both functionalized nanohybrids **1** and **2** indicates that the functionalization is almost of the same degree in both materials, in agreement with TGA data.

The sequence of the structural modification of DWCNTs can also be followed by Raman spectroscopy (785 nm excitation) (Fig. 3 and 4). Pristine DWCNTs exhibit two characteristic bands: the D mode (disordered-induced peak, sp^3 carbon) at around 1305 cm^{-1} and the G mode (1585 cm^{-1}), which corresponds to the stretching mode in graphite (sp^2 carbons). As can been observed in Fig. 3(A) and 4(A), the incorporation of the aryl moiety is traduced as an increase of the D band (which arises from the transformation of the sp^2 to sp^3 carbons), passing from I_D/I_G = 0.02 for pristine **DWCNT** to I_D/I_G = 0.07 for **DWCNT–TMS**. After second functionalization, the incorporation of **ZnPc 3** through the coupling reaction is reflected in the spectrum of **DWCNT–ZnPc 1**. In Fig. 3(B) it is possible to find different peaks arising from **ZnPc 3**: at 1329, 1423 and 1511 cm^{-1} for the peaks relating to the vibrations of pyrrolic ring vibrations; the peak at 1420 cm^{-1} for the C–N stretching vibrations of the phthalocyanine structure as well as peaks at 687 and 748 cm^{-1} associated with the deformation of the macrocycle.[19] These Raman spectra further prove that **DWCNT–Pc 1** has grafted with the **ZnPc 3** moiety successfully.

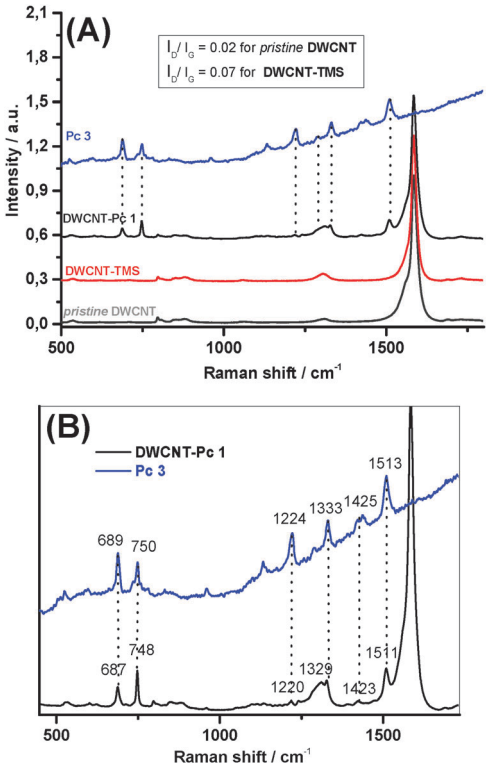

Fig. 3 (A) Zoom of Raman spectra (λ_{exc} = 785 nm) of pristine **DWCNT** (grey), **DWCNT–TMS** (red), **DWCNT–ZnPc 1** (black) and **ZnPc 3** (blue). Intensities have been normalized to the G-band (higher frequency); (B) the inset shows the presence of bands attributed to the ZnPc moiety in **DWCNT–ZnPc 1**.

Analogously, the bands related to **SiPc 4** are found in the Raman spectrum of nanohybrid **2** (Fig. 4): at 1383 and 1195 cm^{-1} (associated with the stretching vibrations of the pyrrole groups), and also the corresponding C–H in-plane vibrations of the benzene groups at 1030 cm^{-1} and 971 cm^{-1}.[20] This fact corroborates the covalent anchoring of **SiPc 4** onto the nanotube surface, in agreement with XPS data.

For both nanohybrids **1** and **2**, the $G^{+\prime}$-band appears at 1586 cm^{-1}, which is downshifted by 2 cm^{-1} as compared to that of the starting DWCNT's peak at 1588 cm^{-1} (Fig. 5). This result demonstrates that the electron-donor moiety linked onto the skeleton of double-walled carbon nanotubes is engaged in intramolecular interactions.[21]

Regarding the radial breathing modes (RBMs) (Fig. 6), comparison of the spectra before and after Tour reaction shows that the RBM bands for the outer walls are reduced in their intensities, whereas the inner wall peaks are hardly affected. The retention of the inner tube suggests that the Tour reaction has a high selectivity on the outer walls of DWCNTs.[5a]

To further demonstrate the anchoring of the **Pcs** on the nanotube skeleton, we employed an atomic force microscopy imaging (AFM) to visualize the height increment of the materials. As shown in Fig. 7, while starting DWCNTs had an average height of ~2 nm (see Fig. S9, ESI†), after grafting the phthalocyanine moiety, the height increased to 3.9 nm (Fig. 7a) for **ZnPc 3** and 4.2 nm in the case of **4** (Fig. 7b); these height increments agree

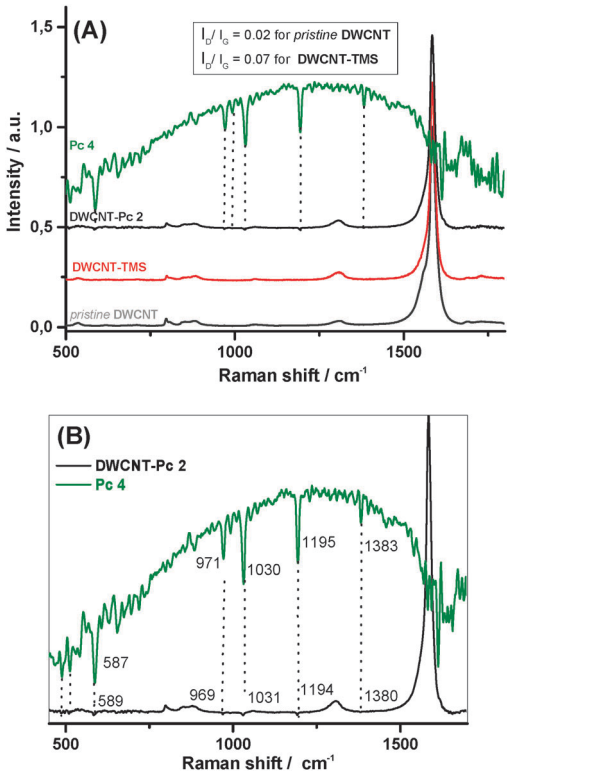

Fig. 4 (A) Zoom of the Raman spectra (λ_{exc} = 785 nm) of pristine **DWCNT** (grey), **DWCNT–TMS** (red), **DWCNT–SiPc 2** (black) and **SiPc 4** (green). Intensities have been normalized to the G-band (higher frequency); (B) the inset shows the presence of bands attributed to SiPcs in **DWCNT–SiPc 2**.

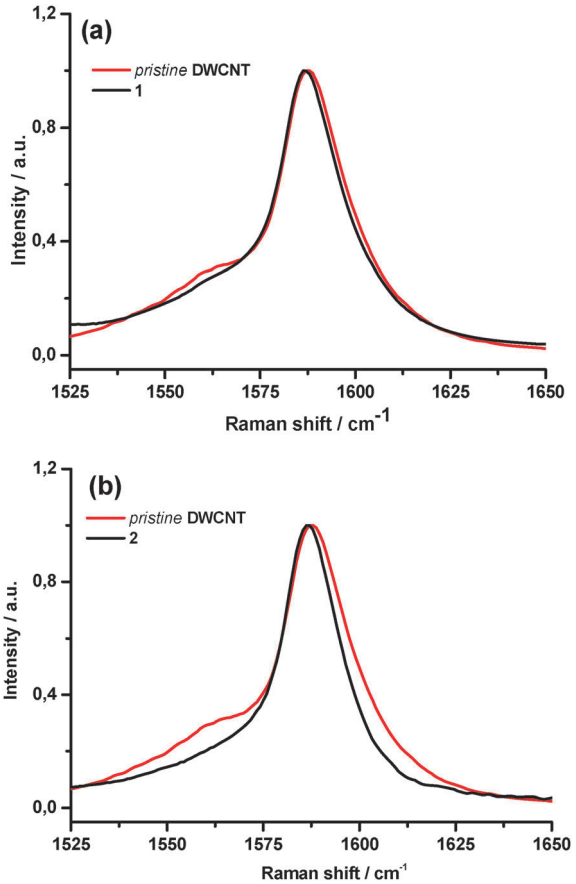

Fig. 5 G-band region (λ_{exc} = 785 nm) of (a) pristine DWCNT in comparison with nanohybrid **1** and (b) pristine DWCNT in comparison with nanohybrid **2**.

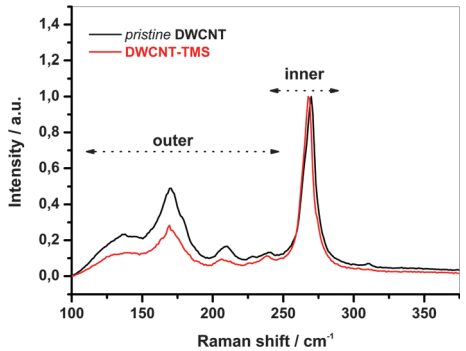

Fig. 6 Comparative Raman spectrum from the RBM zone (785 nm excitation) of pristine **DWCNT** (black), **DWCNT–TMS** (red). Arrows indicate the Raman shift regions where RBMs of the outer and inner tubes are observed.

well with the lengths of phthalocyanines estimated from the more stable conformations obtained by means of molecular mechanics (~2 nm for both hybrids).

Concurring with the AFM results, the transmission electron microscopy (TEM) images revealed materials of several nanometers in size decorated with Pcs in **1** and **2** (Fig. 8).

Electrochemical, spectroscopic and photophysical properties

The electrochemical properties of **DWCNT–Pc 1** and **2** materials were studied by Osteryoung square wave voltammetry (OSWV) and compared with the reference compounds **ZnPc 5** and **SiPc 4** respectively in benzonitrile solution (Table 2). In the nanohybrids, the first oxidation potentials are positively shifted by 60 mV in the case of **1**, and 20 mV for **2** respectively, relative to this corresponding phthalocyanine reference. Moreover, the reduction of the DWCNTs has changed and became a broad signal by the presence of the phthalocyanines and second oxidation and reduction processes of the phthalocyanines are influenced by the presence of the DWCNTs in the hybrids **1** and **2**. The second oxidation of Pcs is not detected due to the interaction of the Pcs with the DWCNTs. In addition, the same interaction affects the Pcs redox potential (see Fig. S10 and S11, ESI†). This suggests that the intramolecular interactions between the electroactive moieties are stronger in the fully conjugated **DWCNT–ZnPc 1** than in the non-conjugated **DWCNT–SiPc 2** hybrid.

The presence of covalent bonded Pcs molecules in **DWCNT–Pc 1** and **2** was further supported by the spectroscopic study using UV-vis spectroscopy (recorded in DMF, PhCN and THF). The absorption spectra of the hybrids **DWCNT–ZnPc 1** and **ZnPc 5** and **DWCNT–SiPc 2** and **SiPc 3** are compared in Fig. 9a and b respectively. The UV-vis spectrum of **ZnPc 5** recorded in THF exhibits a typical metallophthalocyanine Q band, which

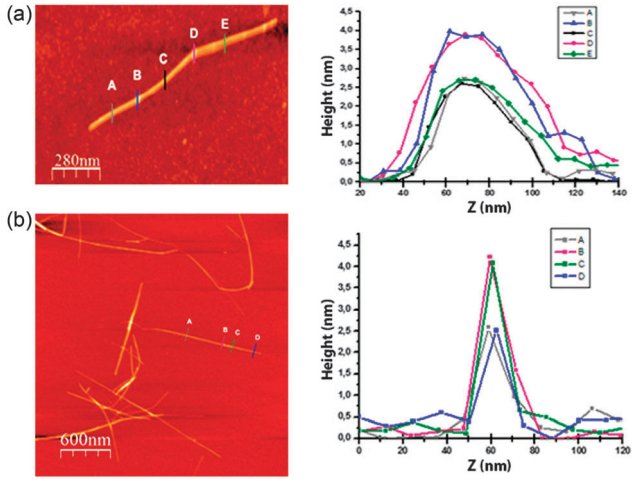

Fig. 7 AFM topographic images of (a) **DWCNT–ZnPc 1** and (b) **DWCNT–SiPc 2** prepared by drop casting on a silicon wafer from a SDBS/water solution.

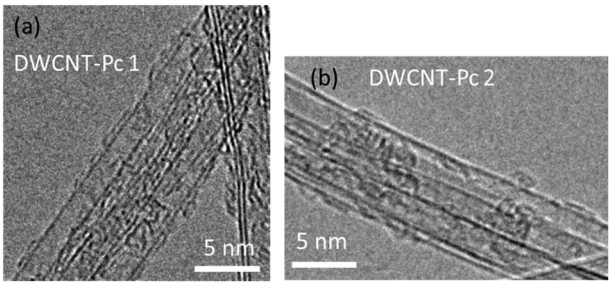

Fig. 8 TEM images of (a) **DWCNT–ZnPc 1** and (b) **DWCNT–SiPc 2**.

Table 2 Electrochemical data determined by OSWV of carbon nanohybrids **1** and **2**, **ZnPc 5** and **SiPc 4**[a]

Compound	E_{ox1}/V	E_{ox2}/V	E_{red1}/V	E_{red2}/V
DWCNT–ZnPc 1	0.45		−1.46	
ZnPc 5	0.39	0.93	−1.52	−1.95
DWCNT–ZnPc 1	0.36[b]	0.87[b]	−1.44[b]	
ZnPc 5	0.32[b]		−1.48[b]	
DWCNT–SiPc 2	0.56			−1.44
SiPc 4	0.54	1.04	−0.96	−1.48

[a] Obtained in a benzonitrile solution containing 0.1 M $TBAPF_6$ and using $Ag/AgNO_3$ as a reference electrode, glassy carbon as a working electrode and a Pt wire counter electrode. Scan rate is 100 mV s^{-1}. Potentials are referenced to Fc/Fc^+. [b] Data obtained in a THF solution.

splits into two peaks at 691 and 681 nm, due to the inherent asymmetry of the molecule. These bands were slightly bathochromically shifted when the spectrum is recorded in PhCN. In the case of hybrid **1**, the Q-band is observed in both solvents together with a broad absorption from 700 to 800 nm indicating an effective conjugation, through a conjugated ethynylbenzyl linker, between the phthalocyanines and the DWCNTs. This interaction is not observed when the Q-band absorption of **SiPc 4** 696 nm is compared with the Q-band in the hybrid **DWCNT–SiPc 2** centred and 698 nm.

Fig. 10a and b show steady-state fluorescence spectra of **DWCNT–ZnPc 1** and **DWCNT–SiPc 2** hybrids (uncorrected for

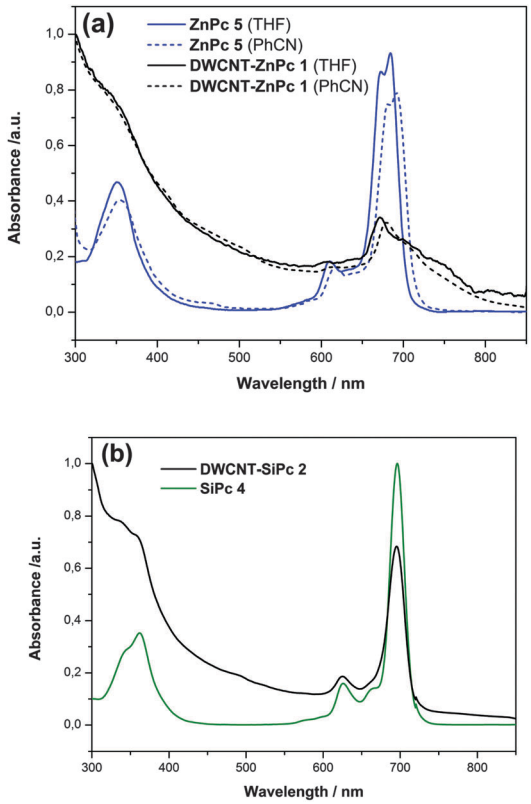

Fig. 9 UV-vis spectra of (a) **ZnPc 5** and **DWCNT–ZnPc 1**, registered in THF and PhCN and (b) **SiPc 4** and **DWCNT–SiPc 2**, registered in PhCN.

DWCNT absorbance) along with their control compounds. **ZnPc 5** in DMF revealed an emission band at 679 nm along with a shoulder band at 742 nm. In the **DWCNT–ZnPc 1** hybrid, the 679 nm band was found to be blue-shifted by 2 nm with quenching of emission intensity as much as 95%. **SiPc 4** in DMF revealed emission at 701 and 775 nm; interestingly, in the hybrid the intense peak was blue-shifted to 684 nm with quenching over 98%. These results reveal interactions between the phthalocyanine sensitizer and DWCNTs. The 17 nm blue-shift of **SiPc 4** emission in the **DWCNT–SiPc 2** hybrid compared to the 2 nm blue-shift in **DWCNT–ZnPc 1** indicates that the **SiPc 4** functionalized *via* axial position interacts better than the **ZnPc 5** functionalized *via* a ring periphery. The phthalocyanine fluorescence quenching in the hybrids could be due to either

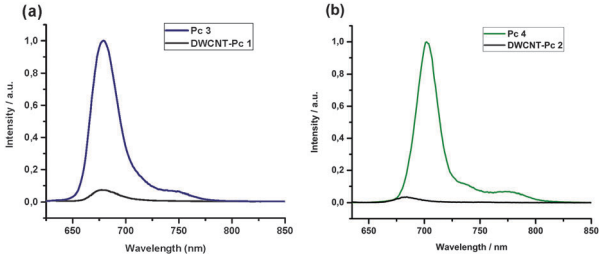

Fig. 10 Steady-state fluorescence spectrum of (a) **ZnPc 5** and **DWCNT–ZnPc 1** hybrid (λ_{ex} = 607 nm) in DMF. (b) **SiPc 4** and **DWCNT–SiPc 2** hybrids (λ_{ex} = 625 nm) in DMF.

ground state complex formation (dark complex *via* inter- or intramolecular association) or dynamic quenching from the singlet excited phthalocyanine.

To clarify this, time resolved fluorescence using the time correlated single photon counting (TCSPC) technique was performed. Both **ZnPc 5** and **SiPc 4** revealed monoexponential decay with lifetimes of 3.15 and 7.32 ns (see Fig. S12 in ESI†), respectively. Our attempts to measure the lifetime of the phthalocyanine in the hybrids to differentiate these two mechanisms were not successful due to very low emission intensity and a relatively high detection limit of the lifetime setup (~200 ps). Further, femtosecond transient absorption studies have been performed to differentiate between the types of interactions and secure any evidence of charge separation in these hybrids.

First, femtosecond transient spectra of the probes, **ZnPc 5** and **SiPc 3**, were recorded. As shown in Fig. S13a (ESI†), upon excitation of **ZnPc 5** (100 fs laser pulses of 400 nm), instantaneous singlet–singlet spectral features were observed with characteristic excited singlet peaks at 438, 478, 560, 630, 730, 840 and 1268 nm accompanied by transient bleaching at 607 and 676 nm, opposite of the absorbance spectral features of **ZnPc 5**.[22] 676 nm also had contributions from stimulated emission of ZnPcs. The singlet features decayed/recovered slowly in accordance with the ZnPc lifetime (3.15 ns) (see Fig. S13b for time profiles of 678 and 1300 nm peaks, ESI†) with a concomitant rise in the triplet features both in the visible and NIR region. The peak at 480 nm could be attributed to the ^{3}ZnPc* state.[23] Similarly, **SiPc 4** immediately after excitation revealed the instantaneous formation of ^{1}SiPc*. Positive peaks at 603, 644, and 838 nm, and a negative peak at 694 nm were observed (Fig. S13c, ESI†). The negative peak corresponded to that of ground state bleaching and stimulated emission of **SiPc 4**. Scanning the spectrum into the near-IR region revealed broad spectral features with peak maxima at 1400 and 1476 nm corresponding to singlet–singlet transition, similar to that observed for ^{1}ZnPc*. The time profile of the 694 nm corresponding to the ground state recovery and decay of the 1476 nm peak are shown in Fig. S13d (ESI†), respectively. These time profiles show slow recovery and decay of the signals in agreement with the relatively long fluorescence life time of SiPcs (7.32 ns).

Excited state interactions in covalently and non-covalently linked phthalocyanine-single walled carbon nanotubes (Pc-SWCNTs) are well known.[23,24] Evidence for the occurrence of electron transfer has been secured from the transient and photocatalytic electron pooling experiments. Fig. 11 shows the femtosecond transient spectra of **DWCNT–ZnPc 1** hybrids in DMF. At an excitation wavelength of 400 nm, the instantaneous formation of a singlet excited state of ZnPcs was observed (spectrum at 0.49 ps). However, instead of slow intersystem crossing, the excited state decayed rapidly at a rate of about 10^{11} s^{-1} revealing efficient excited state interactions between the entities. New negative peaks at 566, 630, 701, 1080, 1206, and 1360 nm, at time constant less than 0.42 ps, were observed. Recovery of the negative peaks was also rapid; in less than 3 ps most of the recovery process of was complete (recovery time constant = 1.22 ps). It is interesting to note that at 850 nm, weak

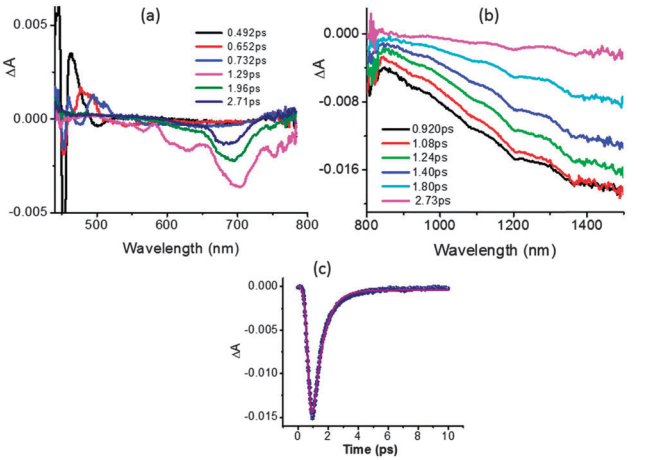

Fig. 11 Femtosecond transient spectra of **DWCNT–ZnPc 1** in DMF at the indicated delay times (a) in the visible and (b) in the near-IR regions. The time profile of the 1200 nm peak is shown in panel (c).

spectral features attributable to ZnPc$^{\bullet+}$ were present (see Fig. 11b). Importantly, these results point out dynamic interactions as the main cause for the observed fluorescence quenching in Fig. 10a.

Similar results were also obtained in the case of the **DWCNT–SiPc 2** hybrid. In this hybrid, initial SiPc singlet excitation was notable (spectrum at 0.32 ps in Fig. 12a) which decayed rapidly at a rate of about 10^{11} s^{-1} revealing strong excited state interactions between SiPcs and DWCNTs. Subsequent relaxation of this peak revealed broad transient minima at 650 nm in the visible region and at 1200, 1370 and 1495 nm in the near-IR region with a time constant of about 0.42 ps (Fig. 12c). Recovery of these peaks was rapid and occurred at a rate constant of 1.16 ps (see Fig. S13c for the time profile, ESI†). Weak spectral features at around 840 nm could be observed in supportive of SiPc$^{\bullet+}$, however, the strong transient minima hampered further analysis of this peak.

Nanosecond transient spectra of the hybrid were also recorded in DMF to seek evidence of charge separation from

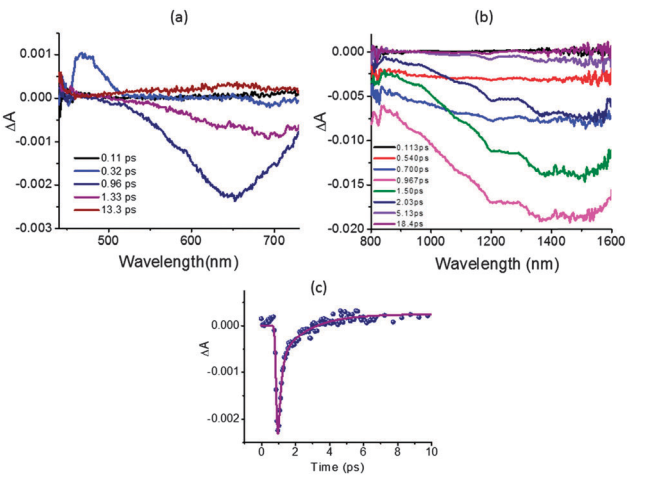

Fig. 12 Femtosecond transient spectra of **DWCNT–SiPc 2** in DMF at the indicated delay times (a) in the visible and (b) in the near-IR regions. The time profile of the 650 nm peak is shown in panel (c).

the ^{3}MPc* (minor product of ^{1}MPc* intersystem crossing, M = Zn and Si). As shown in Fig. S14 (ESI†) for **DWCNT–SiPc 1**, broad spectral features in the 800–870 nm range were observed. In the near-IR region covering the 900–1250 nm range, a few positive features were also observed, supporting a rather weak charge separation process, if any.

The origin of the broad negative peaks in the visible and near-IR region in the case of both hybrids deserves special mention. It is known that sodium dodecylbenzene sulfonate (SDBS) micellar media exfoliate nanotubes effectively from which photoluminescence could be detected.[25] Tsyboulski *et al.* earlier reported photoluminescence studies of DWCNTs in SDBS media and concluded that the observed weak emission is due to the trace amounts of SWCNTs[26] present in the sample. The photoluminescence of the **DWCNT–ZnPc 1** hybrid in SDBS was recorded as shown in Fig. S15 (ESI†). Although much weak, peaks characteristic of SWCNTs were observed suggesting the presence of trace amounts of SWCNTs[26] in the DWCNTs used in the present study. This suggests that the SWCNTs could be responsible for the transient minima peaks seen in Fig. 11 and 12. In fact, the spectral features and peak minima closely resemble that of Pc-SWCNTs reported earlier.[24] These observations suggest weak charge separation in the **DWCNT–ZnPc 1** and **DWCNT–SiPc 2** hybrids although strong excited state interactions are noticed. It may be mentioned here that Aurisicchio *et al.*[27] made such a conclusion on porphyrin–DWCNT hybrids, which also corroborates our recent study on perylenediimide–DWCNT hybrids.[7]

Experimental

General

Ultra purity DWCNTs (catalog number: XNM-UP-11050, purified grade >98%, length = 2 to 6 μm, diameter distribution 1–3 nm, average diameter: 2 nm) were purchased from XinNano Materials Inc. (www.xinnanomaterials.com) and used without further purification treatment. All chemicals were of reagent-grade, purchased from commercial sources, and used as received, unless otherwise specified. All air-sensitive reactions were carried out under an Ar atmosphere. **ZnPc 3** was prepared following the experimental procedure described elsewhere.[28]

DWCNT–TMS

DWCNTs (50 mg) were first stirred in *N*-methyl-2-pyrrolidone (NMP) for 24 h, followed by sonication for 6 h and then 4-(2-(trimethylsilyl)ethynyl)aniline[29] (1.8 g, 8.3 mmol, 2 eq. C) and isoamyl nitrite (1.3 mL, 10 mmol, 2.4 eq. C). The reaction mixture was stirred at 70 °C for 24 h under Ar. After cooling to room temperature, the crude was filtered over a PTFE (Millipore, 0.1 μm pore) membrane to separate the carbon-based material, which was subsequently sonicated in NMP and centrifuged. The supernatant was separated, ant the solid residue resuspended in NMP, filtered again and was washed consecutively with methanol (MeOH) and dichloromethane (CH_2Cl_2) until the filtrate was clear; finally was dried in a vacuum oven at 40 °C to afford a black solid (57.6 mg) as the product.

Deprotection of DWCNT–TMS

To a dispersion of **DWCNT–TMS** (10 mg, 0.83 mmol) in NMP (15 mL) a solution of tetra-*n*-butylammonium fluoride (TBAF, 1 M in THF) (1.66 mmol) was added. The reaction mixture was stirred under 0 °C argon at room temperature for 3 hours, then filtered on PTFE (Millipore, 0.1 μm pore) membranes and washed consecutively with tetrahydrofurane, MeOH, acetone and CH_2Cl_2, to obtain the corresponding **DWCNT–CCH** as a black solid and used directly for the next step.

General procedure for the synthesis of DWCNT–Pc hybrids

$Pd_2(dba)_3$ (2.09 mg, 2.29 μmol) and $AsPh_3$ (14.09 mg, 0.046 mmol) were dissolved in dry *N*,*N*-dimethylformamide (DMF) (15 mL) and subjected to several vacuum/argon cycles. Then, triethylamine (NEt_3) (0.5 mL) was added and subjected to more vacuum/argon cycles. Finally, **DWCNT–CCH** (10 mg) and the corresponding Pcs (15 mg) were added to the reaction. The suspension was sonicated for 10 minutes and heated at 120 °C for 4 days. After cooling to room temperature, the solid was separated by filtration through a PFTE (Millipore, 0.1 μm pore) membrane and washed extensively with DMF. Sonication and redispersion were repeated with acetone, MeOH and CH_2Cl_2 to remove the rest of the phthalocyanines and solvents; the colorless filtrate was checked by TLC (Thin Layer Chromatography) until the phthalocyanines had disappeared. Finally, the solid was dried overnight in a vacuum oven at 40 °C to afford the corresponding modified **DWCNT–ZnPc 1** and **DWCNT–SiPc 2** (17 mg and 14 mg, respectively).

Summary

In summary, the newly synthesized **DWCNT–ZnPc 1** and **DWCNT–SiPc 2** hybrids with differently positioned phthalocyanines (connected through a ring periphery or through an axial bond) reveal different degrees of ground and excited state interactions between the moieties. The synthetic protocols developed here allowed outer walls of the nanotube functionalization leaving the inner walls intact. With the help of HR-TEM, AFM, TGA, XPS and Raman techniques, it was possible to rationalize the level of functionalization. Evidence for excited state interactions in these hybrids was secured from fluorescence (steady-state and time-resolved) and transient absorption spectral studies, with weak, if any, evidence for charge separation. The presence of trace amounts of SWCNTs in the hybrids was witnessed from near-IR photoluminescence and transient absorption studies. Further studies to improve charge separation, photocatalytic activities and organic photovoltaic device characterization of DWCNT and SWCNT derived donor–acceptor hybrids are in progress in our laboratories.

Acknowledgements

This research was financially supported by the Spanish Ministry of Economy and Competitiveness (Mineco) of Spain (CTQ2011-26455, CTQ2013-48252-P and CTQ2014-55798-R), Generalitat Valenciana (GVA) (Prometeo 2012/010), Junta de Comunidades

de Castilla-La Mancha (PEII-2014-014-P) and the US-National Science Foundation (Grant No. 1401188 to FD). LMA and DM thank to Mineco and GVA respectively for FPI grants.

Notes and references

1 (*a*) D. Jariwala, V. K. Sangwan, L. J. Lauhon, T. J. Marks and M. C. Hersam, *Chem. Soc. Rev.*, 2013, **42**, 2824–2860; (*b*) K. Dirian, M. A. Herranz, G. Katsukis, J. Malig, L. Rodriguez-Perez, C. Romero-Nieto, V. Strauss, N. Martin and D. M. Guldi, *Chem. Sci.*, 2013, **4**, 4335–4353; (*c*) C. J. Shearer, A. Cherevan and D. Eder, *Adv. Mater.*, 2014, **26**, 2295–2318; (*d*) A. Stergiou, G. Pagona and N. Tagmatarchis, *Beilstein J. Nanotechnol.*, 2014, **5**, 1580–1589; (*e*) G. Bottari, G. de la Torre and T. Torres, *Acc. Chem. Res.*, 2015, **48**, 900–910.

2 (*a*) W. Lu, M. Zu, J.-H. Byun, B.-S. Kim and T.-W. Chou, *Adv. Mater.*, 2012, **24**, 1805–1833; (*b*) M. F. L. De Volder, S. H. Tawfick, R. H. Baughman and A. J. Hart, *Science*, 2013, **339**, 535–539.

3 (*a*) S. K. Das, A. S. D. Sandanayaka, N. K. Subbaiyan, M. E. Zandler, O. Ito and F. D'Souza, *Chem. – Eur. J.*, 2012, **18**, 11388–11398; (*b*) R. Martín, F. J. Céspedes-Guirao, M. de Miguel, F. Fernández-Lázaro, H. García and Á. Sastre-Santos, *Chem. Sci.*, 2012, **3**, 470–475; (*c*) M. E. Lipińska, S. L. H. Rebelo, M. F. R. Pereira, J. L. Figueiredo and C. Freire, *Mater. Chem. Phys.*, 2013, **143**, 296–304; (*d*) P. d'Ambrosio, M. Carchesio, N. d'Alessandro, G. de la Torre and T. Torres, *Dalton Trans.*, 2014, **43**, 7473–7479.

4 (*a*) J. Bartelmess, B. Ballesteros, G. de la Torre, D. Kiessling, S. Campidelli, M. Prato, T. Torres and D. M. Guldi, *J. Am. Chem. Soc.*, 2010, **132**, 16202–16211; (*b*) C. Backes, F. Hauke and A. Hirsch, *Adv. Mater.*, 2011, **23**, 2588–2601; (*c*) J. K. Sprafke, S. D. Stranks, J. H. Warner, R. J. Nicholas and H. L. Anderson, *Angew. Chem., Int. Ed.*, 2011, **50**, 2313–2316; (*d*) A. S. D. Sandanayaka, N. K. Subbaiyan, S. K. Das, R. Chitta, E. Maligaspe, T. Hasobe, O. Ito and F. D'Souza, *ChemPhysChem*, 2011, **12**, 2266–2273; (*e*) A. De Juan, Y. Pouillon, L. Ruiz-González, A. Torres-Pardo, S. Casado, N. Martín, Á. Rubio and E. M. Pérez, *Angew. Chem., Int. Ed.*, 2014, **53**, 5394–5400.

5 (*a*) A. A Green and M. C. Hersam, *ACS Nano*, 2011, **5**, 1459–1467; (*b*) K. E. Moore, D. D. Tune and B. S. Flavel, *Adv. Mater.*, 2015, **27**, 3105–3137.

6 (*a*) M. Kalbac, A. A. Green, M. C. Hersam and L. Kavan, *Chem. – Eur. J.*, 2011, **17**, 9806–9815; (*b*) M. Vizuete, M. J. Gómez-Escalonilla, S. García-Rodriguez, J. L. G. Fierro, P. Atienzar, H. García and F. Langa, *Chem. – Eur. J.*, 2012, **18**, 16922–16930.

7 (*a*) M. Barrejon, S. Pla, I. Berlanga, M. J. Gómez-Escalonilla, L. Martín-Gomis, J. L. G. Fierro, M. Zhang, M. Yudasaka, S. Iijima, H. B. Gobeze, F. D'Souza, Á. Sastre-Santos and F. Langa, *J. Mater. Chem. C*, 2015, **3**, 4960–4969; (*b*) I. Ojeda, M. Barrejón, L. M. Arellano, A. González-Cortés, P. Yáñez-Sedeño, F. Langa and J. M. Pingarrón, *Biosens. Bioelectron.*, 2015, **74**, 24–29.

8 (*a*) *Phthalocyanines: Properties and Applications*, ed. C. C. Leznoff and A. B. P. Lever, VCH, Weinheim, Germany, 1989, vol. 1–4; (*b*) *Phthalocyanines: Materials Synthesis Structure and Function*, ed. N. B. McKeown, Cambridge University Press, Cambridge, 1998.

9 (*a*) F. J. Céspedes-Guirao, L. Martín-Gomis, K. Ohkubo, S. Fukuzumi, F. Fernández-Lázaro and Á. Sastre-Santos, *Chem. – Eur. J.*, 2011, **17**, 9153–9163; (*b*) V. M. Blas-Ferrando, J. Ortiz, L. Bouissane, K. Ohkubo, S. Fukuzumi, F. Fernández-Lázaro and Á. Sastre-Santos, *Chem. Commun.*, 2012, **48**, 6241–6243; (*c*) V. M. Blas-Ferrando, J. Ortiz, K. Ohkubo, S. Fukuzumi, F. Fernández-Lázaro and Á. Sastre-Santos, *Chem. Sci.*, 2014, **5**, 4785–4793.

10 J. Bahr and J. M. Tour, *Chem. Mater.*, 2001, **13**, 3823–3824.

11 A. Aljarilla, J. N. Clifford, L. Pelleja, P. de la Cruz, F. Langa and E. Palomares, *J. Mater. Chem. A*, 2013, **1**, 13640–13647.

12 E. M. Maya, P. Vázquez and T. Torres, *Chem. – Eur. J.*, 1999, **5**, 2004–2013.

13 D. C. Gale and J. G. Gaudiello, *J. Am. Chem. Soc.*, 1991, **113**, 1610–1618.

14 H. Ali and J. E. Van Lier, *Tetrahedron Lett.*, 1997, **38**, 1157–1160.

15 (*a*) H. P. Boehm, *Carbon*, 2002, **40**, 145–149; (*b*) M. Vizuete, M. J. Gómez-Escalonilla, J. L. G. Fierro, P. Atienzar, H. García and F. Langa, *ChemPhysChem*, 2014, **15**, 100–108.

16 A. Criado, M. Vizuete, M. J. Gómez-Escalonilla, S. García-Rodríguez, J. L. G. Fierro, A. Cobas, D. Peña, E. Guitián and F. Langa, *Carbon*, 2013, **63**, 140–148.

17 A. Jung, R. Graupner, L. Ley and A. Hirsch, *Phys. Status Solidi*, 2006, **243**, 3217–3220.

18 (*a*) K. H. Le Ho, L. Rivier, B. Jousselme, P. Jégou, A. Filoramo and S. Campidelli, *Chem. Commun.*, 2010, **46**, 8731–8733; (*b*) R. L. Arechederra, K. Artyushkova, P. Atanassov and S. D. Minteer, *ACS Appl. Mater. Interfaces*, 2010, **2**, 3295–3302.

19 C. Jennings, R. Aroca, A. Hor and R. Loutfy, *J. Raman Spectrosc.*, 1984, **15**, 34–37.

20 W. M. K. P. Wijekoon and S. P. Karna, *J. Raman Spectrosc.*, 1994, **25**, 949–952.

21 (*a*) V. Straub, A. Gallego, G. de la Torre, T. W. Chamberlain, A. N. Khlobystov, T. Torres and D. M. Guldi, *Faraday Discuss.*, 2014, **173**, 233–256; (*b*) R. Voggu, C. S. Rout, A. D. Franklin, T. S. Fisher and C. N. R. Rao, *J. Phys. Chem. C*, 2008, **34**, 13053–13056.

22 (*a*) S. K. Das, A. Mahler, A. K. Wilson and F. D'Souza, *ChemPhysChem*, 2014, **15**, 2462–2472; (*b*) C. B. KC, G. N. Lim and F. D'Souza, *Nanoscale*, 2015, **7**, 6813–6826.

23 (*a*) F. D'Souza and O. Ito, *Chem. Commun.*, 2009, 4913; (*b*) A. S. D. Sandanayaka, N. K. Subbaiyan, S. K. Das, R. Chitta, E. Maligaspe, T. Hasobe, O. Ito and F. D'Souza, *ChemPhysChem*, 2011, **12**, 2266–2273; (*c*) S. K. Das, N. K. Subbaiyan, F. D'Souza, A. S. D. Sandanayaka, T. Wakahara and O. Ito, *J. Porphyrins Phthalocyanines*, 2011, **15**, 1033–1043; (*d*) R. Chitta, A. S. D Sandanayaka, A. L. Schumacher, L. D'Souza, Y. Araki, O. Ito and F. D'Souza, *J. Phys. Chem. C*, 2007, **111**, 6947–6955; (*e*) F. D'Souza, A. S. D. Sandanayaka and O. Ito, *J. Phys. Chem. Lett.*, 2010,

1, 2586–2593; (*f*) F. D'Souza, S. K. Das, M. E. Zandler, A. S. D. Sandanayaka and O. Ito, *J. Am. Chem. Soc.*, 2011, **133**, 19922–19930.

24 (*a*) J. Bartelmess, A. R. Soares, M. Martínez-Díaz, N. Victoria, G. P. M. S. Miria, A. C. Tome, J. S. Cavaleiro, T. Torres and D. M. Guldi, *Chem. Commun.*, 2011, **47**, 3490–3492; (*b*) J. Bartelmess, B. Ballesteros, G. de la Torre, D. Kiessling, S. Campidelli, M. Prato, T. Torres and D. M. Guldi, *J. Am. Chem. Soc.*, 2010, **132**, 16202–16211; (*c*) U. Hahn, S. Engmann, C. Oelsner, C. Ehli, D. M. Guldi and T. Torres, *J. Am. Chem. Soc.*, 2010, **1322**, 6392–6401; (*d*) G. Bottari, G. de la Torre, D. M. Guldi and T. Torres, *Chem. Rev.*, 2010, **110**, 6768–6816; (*e*) B. Ballesteros, S. Campidelli, G. de la Torre, C. Ehli, D. M. Guldi, M. Prato and T. Torres, *Chem. Commun.*, 2007, 2950–2952; (*f*) B. Ballesteros, G. de la Torre, C. Ehli, G. M. A. Rahman, R. Agulló-Ruedo, D. M. Guldi and T. Torres, *J. Am. Chem. Soc.*, 2007, **129**, 5061–5068; (*g*) D. M. Guldi, A. Gouloumis, P. Vázquez, T. Torres, V. Georgakilas and M. Prato, *J. Am. Chem. Soc.*, 2005, **127**, 5811–5813.

25 J. G. Duque, L. Cognet, A. Nicholas, G. Parra-Vasquez, N. Nicholas, H. K. Schmidt and M. Pasquali, *J. Am. Chem. Soc.*, 2008, **130**, 2626–2633.

26 D. A. Tsyboulski, J.-D. R. Rocha, S. M. Bachilo, L. Cognet and R. B. Weisman, *Nano Lett.*, 2007, **7**, 3080–3085.

27 C. Aurisicchio, R. Marega, V. Corvaglia, J. Mohanraj, R. Delamare, D. A. Vlad, C. Kusko, C. A. Dutu, A. Minoia, G. Deshayes, O. Coulembier, S. Melinte, P. Dubois, R. Lazzaroni, N. Armaroli and D. Bonifazi, *Adv. Funct. Mater.*, 2012, **22**, 3209–3222.

28 E. M. Maya, P. Vázquez and T. Torres, *Chem. Commun.*, 1997, 1175–1176.

29 J.-J. Hwang and J. M. Tour, *Tetrahedron*, 2002, **58**, 10387–10405.